

Mid-infrared [NeII] line emission from the nucleus of NGC 253

Torsten Böker

Space Telescope Science Institute, 3700 San Martin Drive, Baltimore, MD 21218, U.S.A.

Alfred Krabbe

Max-Planck-Institut für extraterrestrische Physik, Garching, Germany

DLR, Institute of Space Sensor Technology, Rudower Chaussee 5, Berlin, Germany

John W.V. Storey

University of New South Wales, School of Physics, Sydney, Australia

Received Jan. 14, 1998; accepted March 6, 1998

ABSTRACT

We report on mid-infrared (MIR) continuum and line emission mapping of the nucleus of NGC 253. The data, with a resolution of $1''.4$, reveal a double-peaked arc-like [NeII] emission region. Comparison with published data shows that the [NeII] arc is centered on the nucleus of the galaxy. The brightest [NeII] source coincides with the infrared continuum peak. The interpretation of these results is complicated by the edge-on orientation of NGC 253, but a self-consistent explanation is starformation triggered by dynamical resonances in a barred potential.

Subject headings: infrared: ISM: lines and bands — galaxies: starburst — galaxies: individual (NGC 253)

1. Introduction

The prototypical starburst galaxy NGC 253 is a highly inclined ($i=78^\circ$, Pence 1981) disk galaxy at a distance of about 3 Mpc (Tully 1988). The view towards its inner region is heavily obscured, and the exact location of its nucleus has been the matter of some debate. The astrometry of the various infrared sources in the central $10''$ has been discussed in detail by Kalas & Wynn-Williams (1994, hereafter KW94) in the near-infrared and Keto *et al.* 1993 in the mid-infrared. From their $\approx 1''$ resolution H, K, L, and M observations, KW94 conclude that the brightest source in all the maps (their peak 1) lies at R.A.(1950)= $00^h45^m5^s.62$, Decl.(1950)= $-25^\circ33'40''.2$. This position is in very good agreement with that of the emission peak at MIR wavelengths as determined by Keto *et al.* (1993) at $10\ \mu\text{m}$ from astrometric methods and Piña *et al.* (1992) from low-level contour fitting to published maps with lower resolution. It is safe to assume that the location of peak 1 is independent of wavelength up to $20\ \mu\text{m}$, enabling us to adopt the above coordinates for the continuum peak in our maps.

Peak 1 is not connected to any of the strong radio point sources found at 2 cm by Turner & Ho (1985, hereafter TH85) and 6 cm by Ulvestad & Antonucci (1991) and Antonucci & Ulvestad (1988). The radio sources are highly aligned along the major axis of NGC 253 at P.A. 51° . All of them are most likely either radio supernovae or HII regions, based on their spectral index. The only exception is the source TH 2 in TH85, a powerful flat spectrum radio source that they proposed to be the nucleus of NGC 253. TH85 argue that because of its high radio luminosity ($10^4 L_\odot$) and its unique location at the center of a synchrotron disk this source probably is a compact synchrotron source, similar to those observed in active galactic nuclei (AGNs). It lies close to a secondary MIR peak (peak 2) $\approx 2''.2$ northeast of peak 1 (Piña *et al.* 1992, Keto *et al.* 1993). However, as we will show, the radio nucleus is most likely not identical with any characteristic infrared source. This view was strongly supported from $0.5''$ resolution NIR color maps by Sams *et al.* (1994). Their maps were referenced to other observations by cross-correlation of low level contours and show that the radio nucleus TH 2 coincides with an extinction maximum of $A_V \geq 24$. In addition, KW94 show that the exact position of peak 2 is wavelength dependent in the sense that for J, H, K observations it lies $\approx 1''$ further east than in M-band.

The physical nature behind the various infrared sources is uncertain. For example, according to Forbes *et al.* (1993), the emission of the Br γ -line at $2.17\ \mu\text{m}$ is strongest at peak 1. On the other hand, KW94 show that peak 1 has a low PAH-feature/continuum emission ratio. Since PAH emission is usually indicative of ongoing star formation, KW94 argue against peak 1 being an intense starburst which would be the natural

explanation for the Br γ emission. To investigate this matter further, we have observed NGC 253 at MIR wavelengths, both in continuum and line emission. The forbidden ${}^2P_{3/2} - {}^2P_{1/2}$ transition of singly ionized Neon at 12.81 μm traces the photoionization regions of hot stars and thus carries similar information than e.g. Br γ , but at a much lower extinction: $A_{2.17\mu\text{m}} \approx 2.5 \cdot A_{12.8\mu\text{m}}$ (Lutz *et al.* 1996, Genzel *et al.* 1998).

In the next section we will describe how the data were obtained. We also discuss the special observing techniques in the MIR and their implications on data reduction. We present the results of our observations in Sec. 3 and interpret them in Sec. 4.

2. Observations and data reduction

Our observations were carried out with MANIAC, the Mid- And Near-Infrared Array Camera (Böker *et al.* 1997a) built at the Max-Planck-Institut für extraterrestrische Physik in Garching, Germany. NGC 253 was observed during five nights at the ESO 2.2m telescope in LaSilla, Chile in October 1996. The average seeing was below 1'', therefore the data have a spatial resolution defined by the diffraction limit of about 1''.4.

We used three narrow band filters ($\frac{\Delta\lambda}{\lambda} \approx 0.015$) centered on the [NeII] line (12.81 μm) and two continuum positions shortwards (12.62 μm) and longwards (13.00 μm). This is essential for accurate continuum subtraction, because strong Silicate absorption features and emission from polycyclic aromatic hydrocarbon (PAH) make it difficult or even impossible to determine the continuum emission underlying the [NeII] line from N-band photometry. The mean of the two continuum images should represent the emission underlying the [NeII], its subtraction from the 12.81 μm map then reveals the distribution of the [NeII] emission. The total on-source integration time was about 9600 s on the [NeII] filter and 4800 s on each of the two continuum filters.

Due to the high thermal background of the atmosphere at wavelengths around 10 μm , rapid readout of the detector, chopping of the telescope secondary, as well as frequent beam switching is essential. We typically used a chop amplitude of 15'' so that the source remained on the MANIAC detector all the time. The correct telescope movement for the beam switch was defined with high precision by alternate guiding on each of the two (chopped) images of a nearby guide star.

The sky signal through the filters allowed single frame integration times of 80 ms before saturating the detector. Frames taken immediately after the chop movement were discarded because of the settling

time of the secondary. After 1 min, the data (two sums of about 375 frames for each chop position) were transferred to the MANIAC PC and the beam switch was performed. After subtraction of the two beams, the residual background emission in our data is typically reduced by a factor of 10^5 , as can be determined from empty regions in our images.

During the course of the night one gathers many such exposures, which have to be coadded. Because of refraction by the atmosphere, the source slowly changes position on the detector as the zenith distance changes. We correct for this drift by coadding a few exposures both at the beginning and the end of the observations to increase the signal-to-noise ratio, and determining the centroids of the well-defined emission peak. Their difference in position gives the drift over this timeline. Assuming it to be linear with time, we can estimate the drift per exposure and correct each before coadding them.

The chop amplitude and direction, required for the correct overlay of the three source images on the detector, was accurately determined by observing a point source in an identical way, and fitting Gaussians to its three images. Finally, the resulting maps were calibrated for (slightly) different filter transmissions and a mean image for each filter was generated from the data of the individual nights. Because the $12.81\mu\text{m}$ filter showed a ghost reflection during the October 1996 run, the filter maps had to be deconvolved with their point spread functions (PSF) before subtraction. We used a CLEAN algorithm (Högbom 1974) with observations of reference stars as the PSF for each filter. Since the observations described here are diffraction limited, the PSF is much more stable and the deconvolution more reliable than is normally the case.

Flux calibration of our data was performed by assuming that the $12.8\mu\text{m}$ flux density of the nearby star β Ceti is 53 Jy. This number was extrapolated from the $12\mu\text{m}$ IRAS flux and a blackbody temperature of 4200 K. The flux density inside a $5''.5$ aperture at $12.8\mu\text{m}$ is 17 Jy which should be compared to the value of 11.2 Jy given by Rieke & Low (1975) in the same aperture at $12.6\mu\text{m}$. The total flux density in our map is 35 Jy, about a factor of 2.5 higher than the result of Keto *et al.* (1993), measured at $12.5\mu\text{m}$. On the other hand, the [NeII] flux we derive from the central $7''.6$ is $2 \cdot 10^{-14} \text{ W/m}^2$, roughly 60% of the result by Roche *et al.* (1991). The data thus seem to agree to some extent, although it should be stressed that a direct comparison between various data sets is problematic because of the differences in filter passbands and bandwidths. This is especially true in the MIR since this regime is rich in spectral features.

3. Results

3.1. Morphology of the continuum and [NeII] emission

The results of the above data reduction are presented in Fig. 1 (Plate 1). We show in panel A) the “raw” 12.81 μm filter map before deconvolution with the PSF and in B) the deconvolved 12.81 μm map. Panels C) and D) contain the two deconvolved continuum maps at 12.62 μm and 13.00 μm . Finally, panel E) shows the resulting [NeII] line map, calculated as described in Sec. 2. The continuum maps show a good overall agreement with other MIR maps at comparable resolution (Piña *et al.* 1992, Keto *et al.* 1993), although there are differences in the detailed emission morphology. This emphasizes our point that a reliable continuum subtraction is only possible with narrow band continuum filters neighboring the emission line.

Since both the strongest two continuum sources and the elongated emission structure along the major axis of the NGC 253 disk at P.A. 51° (Pence 1981) are easily identified, we can safely adopt the astrometry and terminology used by KW94 (Sec. 1). For the remainder of this paper, we will identify our strongest continuum source with peak 1 and the secondary continuum source with peak 2, keeping in mind that at NIR wavelengths peak 2 is offset by $\approx 1''$ to the east.

The most striking result of the [NeII] map is that the emission forms a double-peaked, arc-like structure. The brightest source coincides with peak 1, adding to the evidence that it is indeed powered by a burst of star formation. The opposite end of the arc seems to coincide with peak 2, but is somewhat elongated in E-W direction. The [NeII] morphology is in excellent agreement with the $\text{Br}\gamma$ map of Forbes *et al.* (1993).

It is important that the [NeII] emission from the central $\approx 5''$ is aligned with the major axis of the NGC 253 optical disk. In Fig. 2 we show again contour plots of the [NeII] and continuum emission to demonstrate its relative orientation. The line of nodes at P.A. 51° is indicated by the dashed line. The dotted line shows the orientation of the NIR bar detected first by Scoville *et al.* (1985). The [NeII] morphology and its relation to the NIR bar will be further discussed in Sec. 4.

3.2. The radio nucleus

Adopting the coordinates of peak 1 of KW94, we can relate our maps to the astrometry at longer wavelengths. In Fig. 2, we have marked the location of the compact radio sources of TH85 on both the [NeII] and the continuum emission. As can be seen, the major axis of the [NeII] emission coincides well with the radio axis. The radio nucleus TH 2 - or extinction peak according to Sams *et al.* (1994) - does fall on none of the [NeII] or continuum peaks. Rather, TH 2 lies inside the arc-like [NeII] emission region.

This supports the view of TH85 that TH 2 is most likely not an HII region, but a synchrotron source in the dynamical center of NGC 253. All other radio point sources are distributed rather randomly in the plane of the [NeII] emission, supporting the idea of them being radio supernovae (TH85).

To summarize, the location of the nucleus of NGC 253 lies in the center of the [NeII] emission arc, about $2''.2$ northeast of peak 1 in a region with high extinction.

4. Interpretation and discussion

4.1. The bar in NGC 253

From $10''$ resolution K-band imaging, Scoville *et al.* (1985) find a prominent NIR bar at P.A. 68° . However, the NIR continuum of the central $\approx 10''$ in all high resolution NIR maps (e.g. Forbes *et al.* 1993, KW94, Sams *et al.* 1994) is oriented at P.A. 51° , roughly parallel to the major axis of the optical disk. This change in orientation is also visible as an isophote twist in Scoville *et al.* (1985) and all MIR maps (Piña *et al.* 1992, Keto *et al.* 1993, Fig. 2). What is the reason for this behavior? From kinematical studies of the CS(2-1) line at 98 GHz, Peng *et al.* (1996) have tried to answer this question. They derived a model for the dynamical processes in the center of NGC 253. In short, they find five prominent CS emission spots. The two innermost spots are aligned along the axis of the radio knots, i.e. the major axis of NGC 253. They are separated by $\approx 3''$ and positioned symmetrically on either side of the radio nucleus. Two other knots lie again symmetrically to the nucleus, but are aligned with the large scale NIR bar. Their observations are well explained by a rotating gas torus around the dynamical center of NGC 253. The torus is the response of the viscous molecular gas to the potential of the NIR stellar bar. Gas clouds in the inner $\approx 10''$ move along elliptical x_2 orbits whose major axis is aligned perpendicular to the bar (Athanasoula 1992a,b). At the inclination of NGC 253, these orbits appear to be oriented parallel to the major axis of the optical disk as demonstrated in Fig. 5 of Peng *et al.* (1996). The gas clouds outside of $\approx 10''$ move on x_1 orbits, their major axis being aligned with the bar. The existence of x_2 orbits depends on the presence of at least one Inner Lindblad Resonance (ILR). For the case of NGC 253, Arnaboldi *et al.* (1995) have shown that there are in fact two ILRs, one at a radius of $25''$, the other close to the nucleus. It is at the inner ILR, where the orientation of the dominant orbits changes from x_2 to x_1 (e.g. Telesco & Decher 1988). Because of orbit crowding, massive star formation occurs predominantly at the apocenters of the x_2 orbits (Athanasoula 1992b), oriented symmetrically on either side of the nucleus. Therefore, Peng *et al.* (1996) interpret their CS results as evidence for a rotating torus of dense gas around the radio nucleus TH 2. These results are in

agreement with observations of other tracers of high density gas like HCN (Paglione *et al.* 1995).

4.2. The [NeII] arc - a starformation ring

Based on their model, Peng *et al.* (1996) predict that higher resolution line mapping should prove that gas emission from the central $10''$ (145 pc) of NGC 253 is aligned with the radio knots rather than with the optical disk. In that context, our results provide an independent confirmation of this scenario. Firstly, the [NeII] emission is well aligned with the radio knots (Figs. 1 (Plate 1) and 2). Secondly, based on the structure of the [NeII] emission, we also confirm the distribution of the star forming material in a ring around the radio nucleus. The ring has a rotation velocity of ≈ 60 km/s as seen in the CS data by Peng *et al.* (1996), the western side moving away from the observer. Unfortunately, our observations are unable to resolve the velocity structure of the [NeII], this has to await higher resolution line mapping, e.g. with a cryogenic Fabry-Perot interferometer.

Our data only show weak emission from the southeastern half of the ring. On the other hand, the [FeII] map of Forbes *et al.* (1993) does show emission from this region (their source B). Thus, we favor the interpretation of the double-peaked morphology as a starburst ring with a diameter of $\approx 4''$ (60 pc). The total observed flux from a circular aperture with $1''.4$ (20 pc) diameter centered on peak 1 is $1.7 \cdot 10^{-15}$ W/m². After dereddening with $A_V = 24$ (Sams *et al.* 1994) in a mixed case scenario, this corresponds to $7.7 \cdot 10^5 L_\odot$ ¹.

With the conversion factor $\frac{L_{\text{Ly}\alpha}}{L_{[\text{NeII}]}} = 64$ (Genzel *et al.* 1998), the intrinsic Lyman-continuum luminosity is $4.9 \cdot 10^7 L_\odot$. This value should be used with caution given its uncertainties, but it compares well to other bright star forming regions like the core of 30 Doradus in the LMC (Brandl *et al.* 1996) or the brightest SFR in the gaseous ring of IC 342 (Böker *et al.* 1997b). This supports the view that the [NeII] emission probably stems from individual giant molecular clouds (GMCs) that actively form stars and are located in a ring at the ILR. We will extend the comparison to a similar structure in IC 342 in the next section.

¹We have adopted $A_{12.8\mu\text{m}} = 0.04 \cdot A_V$ (Genzel *et al.* 1998)

4.3. NGC 253 and IC 342 - two of the same kind?

It is interesting to note the close similarities between NGC 253 and IC 342, another nearby late type spiral. Böker *et al.* (1997b) describe the dynamical processes in the central 100 pc of IC 342 as derived from NIR integral field spectroscopy. Table 1 compares the two galaxies. The dynamical processes and the morphology of the molecular gas are almost identical. This was also noted by Paglione *et al.* (1995). One important difference, however, is that IC 342 does not house a central synchrotron source. In fact, in the case of IC 342, there is no radio emission from the dynamical center (Turner & Ho 1983). Rather, it is occupied by a cluster of young red supergiants that dominate the NIR continuum. For NGC 253, there is no obvious NIR component at the location of the radio nucleus, but the edge-on orientation and patchy extinction might complicate its detection. Both the diameter and rotation velocity of the molecular rings are very similar. This adds to the increasing evidence that stellar bars and small star formation rings on scales of 50-100 pc are a common feature in late type spirals. This points to an evolutionary connection between spirals of different Hubble type, as suggested by Pfenniger *et al.* (1994).

5. Summary

We have reported on MIR line and continuum mapping of the central 200 pc of NGC 253. The main results can be summarized as follows:

- 1) The continuum maps confirm that the nucleus of NGC 253 is not identified with any strong IR source.
- 2) The [NeII] map reveals two peaks separated by about $4''$ and connected by an arc-shaped emission region.
- 3) The nucleus lies inside the [NeII] arc.
- 4) We interpret the morphology of the [NeII] map as evidence for a bar-triggered starformation ring with a diameter of 50 pc, similar to that seen in IC 342.

It is a pleasure to thank Thomas Lehmann for his invaluable help before, during, and after the campaign. We are indebted to the ESO 2.2m-team for their continuous support, and to Rolf Chini and Craig Smith who helped a great deal with the observations. We also would like to acknowledge Thomas Ott for his expertise on deconvolution algorithms, and the anonymous referee whose comments led us to re-examine the point spread function and thereby substantially improve this paper. JWVS thanks the Alexander von Humboldt Stiftung for their support during the development of MANIAC, and the

Australian DIST for travel support.

REFERENCES

- Antonucci, R. R. J. & Ulvestad, J. S. 1988, *ApJ*, 330, L97
- Arnaboldi, M., Capaccioli, M., Cappellaro, E., Held, E. V., & Koribalski, B. 1995, *AJ*, 110, 199
- Athanassoula, E. 1992a, *MNRAS*, 259, 328
- Athanassoula, E. 1992b, *MNRAS*, 259, 345
- Böker, T., Storey, J. W. V, Krabbe, A., & Lehmann, T. 1997a, *PASP*, 109, 827
- Böker, T., Förster-Schreiber, N. M., & Genzel, R. 1997b, *AJ*, 114, 1883
- Brandl, B., *et al.* 1996, *ApJ*, 466, 254 & Wild, W. 1990, *ApJ*, 348, 434
- Forbes, D. A., Ward, M. J., Rotatiuc, V., Blietz, M., Genzel, R., Drapatz, S., van der Werf, P., & Krabbe, A. 1993, *ApJ*, 406, L11
- Genzel, R. *et al.* 1998, accepted for publication in *ApJ*
- Högbom, J. A. 1974, *A&AS*, 15, 417
- Kalas, P. & Wynn-Williams, C. G. 1994, *ApJ*, 434, 546
- Keto, E., Ball, R., Arens, J., Jernigan, G., Meixner, M., Skinner, C., & Graham, J. 1993, *ApJ*, 413, L23
- Lutz, D., *et al.* 1996, *A&A*, 315, L269
- Madore, B. F. & Freedman, W. L. 1992, *PASP*, 104, 362
- McCall, M. L. 1989, *AJ*, 97, 1341
- Newton, K. 1980, *A&A*, 191, 169
- Paglione, T. A. D., Tomaka, T., & Jackson, J. M. 1995, *ApJ*, 454, L117
- Pence, W. D. 1981, *ApJ*, 247, 473
- Peng, R., Zhou, S., Whiteoak, J. B., Lo, K. Y., & Sutton, E. C. 1996, *ApJ*, 470, 821
- Pfenniger, D., Combes, F. & Martinet, L. 1994, *A&A*, 285, 79

- Piña, R. K., Jones, B., Puetter, R. C., & Stein, W. A. 1992, *ApJ*, 401, L75
- Roche, P. F., Aitken, D. K., Smith, C. H., & Ward, M. J. 1991, *MNRAS*, 248, 606
- Rieke, G. H. & Low, F. J. 1975, *ApJ*, 197, 17
- Sams, B. J. III., Genzel, R., Eckart, A., Tacconi-Garman, L. E., & Hofman, R. 1994, *ApJ*, 430, L33
- Scoville, N. Z., Soifer, B. T., Neugebauer, G., Young, J. S., Matthews, K., & Yerka, J. 1985, *ApJ*, 289, 129
- Telesco, C. M. & Decher, R. 1988, *ApJ*, 334, 573
- Tully, R. B., 1988, *Nearby Galaxies Catalog* (Cambridge: Cambridge Univ. Press)
- Turner, J. L. & Ho, P. T. P. 1983, *ApJ*, 178, 623
- Turner, J. L. & Ho, P. T. P. 1985, *ApJ*, 299, L77 [TH85]
- Ulvestad, J. S. & Antonucci, R. R. J. 1991, *AJ*, 102, 875

Fig. 1.— MIR maps of the central $15''$ (200 pc) of NGC 253. A) “raw” $12.81\mu\text{m}$ filter map before CLEANing. B) $12.81\mu\text{m}$ filter map after CLEANing. C) $12.62\mu\text{m}$ continuum map after CLEANing. D) $13.00\mu\text{m}$ continuum map after CLEANing. E) [NeII] line map calculated as $B - (C+D)/2$. The resolution in all maps is $1''.4$ The coordinate origin is the continuum peak (peak 1) at $\text{R.A.}(1950)=00^{\text{h}}45^{\text{m}}5^{\text{s}}.62$, $\text{Decl.}(1950)=-25^{\circ}33'40''.2$. The contour levels for the three continuum maps are 4, 8, 12, 16, 20, 30, 40...100% of the peak continuum flux at $12.8\mu\text{m}$ ($1.6 \cdot 10^{-16} \text{ W/m}^2/\square''$), and 6, 12, 18, 24, 30, 40, 50...100% of the peak line flux ($2.3 \text{ Jy}/\square''$) for the [NeII] map.

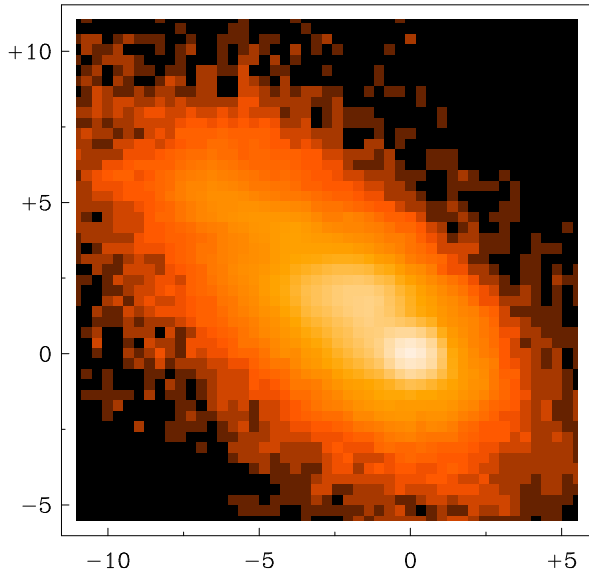
Fig. 2.— $12.8\mu\text{m}$ continuum emission (top) and [NeII] line emission (bottom) from the central $15''$ (200 pc) of NGC 253. The coordinate origin is the continuum peak (peak 1) at $\text{R.A.}(1950)=00^{\text{h}}45^{\text{m}}5^{\text{s}}.62$, $\text{Decl.}(1950)=-25^{\circ}33'40''.2$ (see text for discussion). The resolution in both maps is $1''.4$. Contour levels are 4, 8, 12, 16, 20, 30, 40...100% of the peak flux ($2.3 \text{ Jy}/\square''$) for the continuum and 6, 12, 18, 24, 30, 40, 50...100% of the peak flux ($1.3 \cdot 10^{-15} \text{ W/m}^2/\square''$) for the [NeII] map. The location of the non-thermal radio nucleus TH 2 (coincident with the NIR extinction peak of Sams *et al.* 1994) as well as the thermal 2cm radio point sources of TH85 are marked by the indicated symbols for *Nuc* and *SNR*, resp. The dashed line shows the orientation of x_2 orbits that form the starburst ring. Incidentally, this is identical with the major axis of the optical disk of NGC 253 at P.A. 51° . The dotted line denotes the orientation of the NIR bar at P.A. 68° .

Table 1. NGC 253 and IC 342 - a comparison

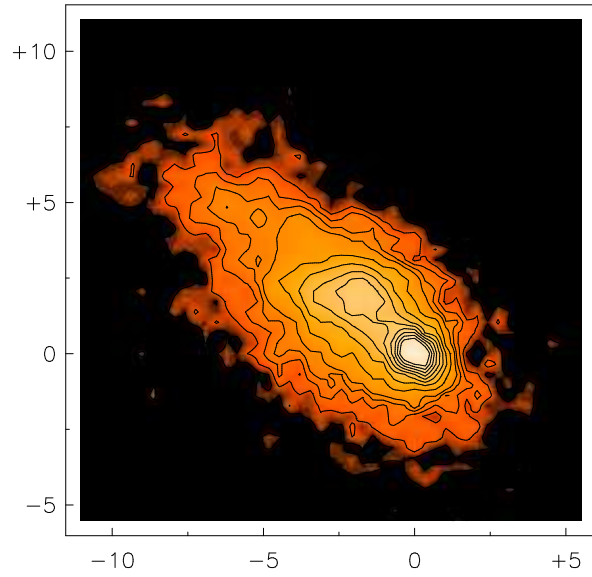
Property	IC 342	NGC 253	Ref.
Distance [Mpc]	1.8	3	1,2
Inclination	25°	78°	3,4
P.A.	39°	51°	3,4
Morph. type	Scd	Sc	5
Radio core	no	yes	6,7
P.A. of NIR bar	0°	68°	8,9
No. of ILR's	1	2	8,10
Ring diameter [pc]	70	60	8,11
L_{Lyc} from brightest SRF [$10^7 L_{\odot}$]	1.7	4.9	8,12

Note. — References: 1) McCall 1989, Madore & Freedman 1992
 2) Tully 1988 3) Newton 1980 4) Pence 1981 5) NASA extragalactic
 database (NED) 6) Turner & Ho 1983 7) Turner & Ho 1985 8)
 Böker *et al.* 1997b 9) Scoville *et al.* 1985 10) Arnaboldi *et al.* 1995
 11) Peng *et al.* 1996, Paglione *et al.* 1995, this work, 12) this work

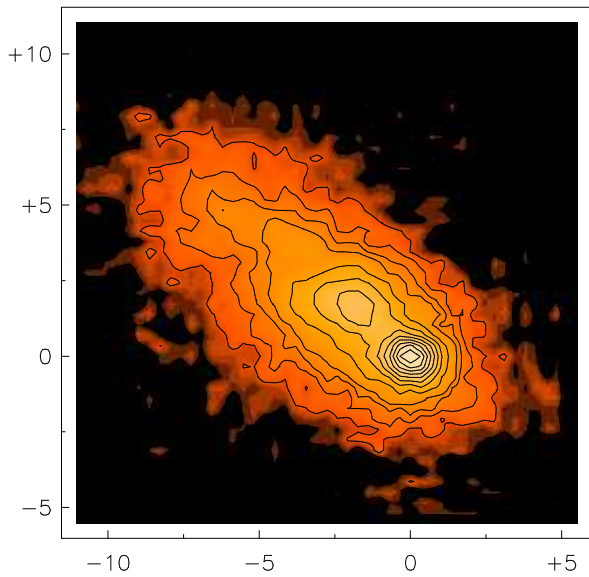
A) 'raw' Continuum + line (12.81 μm)



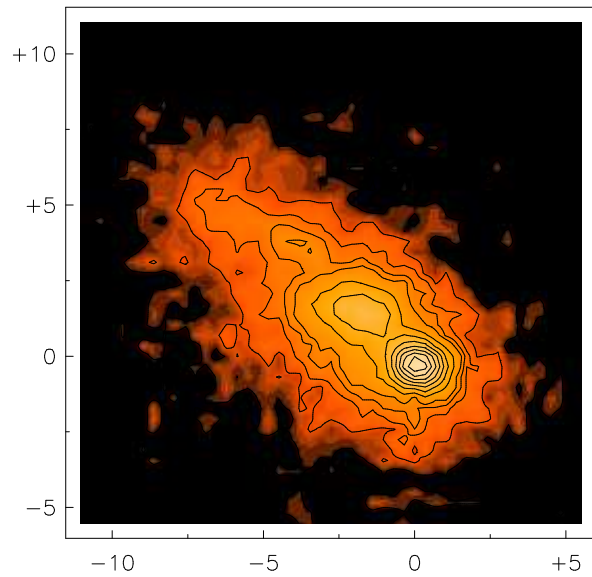
B) CLEANed Continuum+line (12.81 μm)



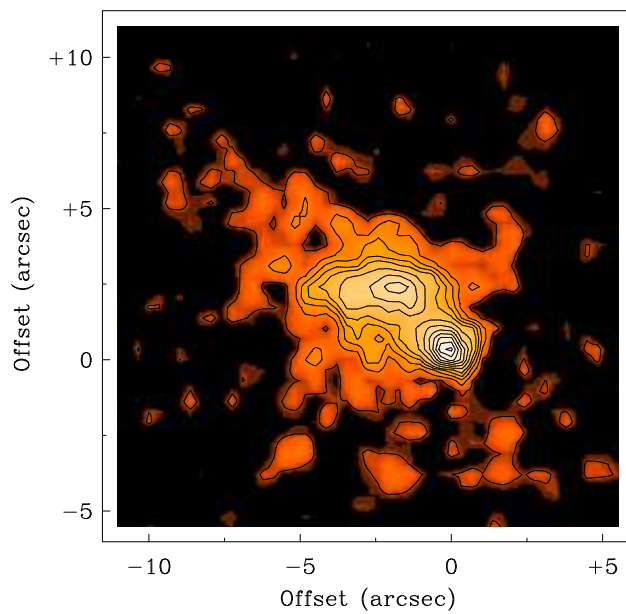
C) CLEANed 12.62 μm -Continuum



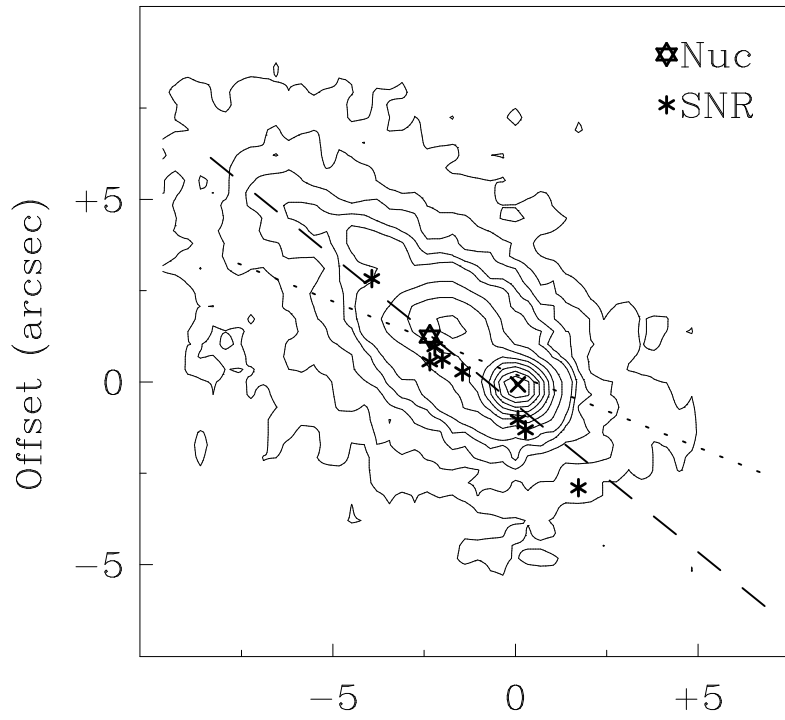
D) CLEANed 13.00 μm -Continuum



E) [NeII] line $(B-(C+D))/2$



12.8 μm -Continuum



[NeII] emission

